 CMES, vol.102, no.6, pp.425-447, 2014

The Boundary Integral Equation for 3D General Anisotropic Thermoelasticity

Y.C. Shiah[1] **and C.L. Tan**[2,3]

Abstract: Green's functions, or fundamental solutions, are necessary items in the formulation of the boundary integral equation (BIE), the analytical basis of the boundary element method (BEM). In the formulation of the BEM for 3D general anisotropic elasticity, considerable attention has been devoted to developing efficient algorithms for computing these quantities over the years. The mathematical complexity of this Green's function has also posed an obstacle in the development of this numerical method to treat problems of 3D anisotropic thermoelasticity. This is because thermal effects manifest themselves as an additional domain integral in the integral equation; this has implications for the numerical modeling in BEM. Difficulties in deriving a true BIE arise, unless some simple representations of the thermal effects are used, such as in the dual reciprocity approach. These approximation schemes, however, have some serious limitations. An integral transformation method to obtain an exact BIE has been successfully employed, but only for isotropy and two-dimensional (2D) general anisotropy. The extension of this scheme to three-dimensional (3D) general anisotropy has remained a very serious challenge. This paper reports on the progress towards this end. By following the same steps as for 2D general anisotropy, and using a double-Fourier series representation of the Green's function first proposed by the authors recently, a true BIE is derived for 3D general anisotropic thermoelasticity. Some numerical results are presented to demonstrate the success of this derivation.

1 Introduction

The boundary element method (BEM) is recognized as an efficient numerical tool for engineering stress analysis with its distinctive feature that only the boundary or

[1] Department of Aeronautics and Astronautics, National Cheng Kung University, Tainan 701, Taiwan, R.O.C.

[2] Department of Mechanical & Aerospace Engineering, Carleton University, Ottawa, Canada K1S 5B6.

[3] Corresponding author. E-mail: choonlai.tan@carleton.ca

surface of the solution domain needs to be discretized. This stems from the analytical transformation of the governing differential equations into a boundary integral equation (BIE). The kernels of the BIE involve the Green's function (or fundamental solution) for displacements and its derivatives. Although the general analytical and numerical formulations of the BEM for isotropic elasticity have been very well established for over three decades, the same cannot be said about the case for general anisotropic elasticity, especially for 3D solids. This is due to the significantly more complex mathematical form of the Green's function and its derivatives.

The Green's function for the displacements in a generally anisotropic, elastic body in three dimensions was first derived by Lifschitz and Rosenzweig (1947). It is not algebraically explicit, but is instead expressed as a line integral around a unit circle with the integrand containing the Christoffel matrix defined in terms of elastic constants. Since then, the re-formulation of this fundamental solution and its derivatives into simpler forms to facilitate their evaluation and more efficient computation has been a focus of numerous researchers. A brief review of this may be found in, e.g., Shiah, Tan and Lee (2008), Tan, Shiah and Lin (2009). In the pioneering work of Wilson and Cruse (1978) on BEM for 3D general anisotropic elastostatics, the Green's function of Lifschitz and Rosenzweig (1947) is employed. In their numerical algorithm, the Green's function and its derivatives required in the integration of the BIE are obtained by interpolation of pre-calculated values from a database that is generated in advance for a given material. This is evidently quite cumbersome; it is less than efficient; and, its accuracy has been questioned for highly anisotropic materials. The development and use of other forms of the Green's function with BEM has also been proposed by, e.g., Tonon, Pan and Amadei (2001), Phan, Gray and Kaplan (2004), Wang and Denda (2007), Tan, Shiah and Lin (2009).

Of significance to note here is that in Ting and Lee (1997), a fully algebraic form of the 3D Green's function for general anisotropic elasticity, expressed in terms of Stroh's eigenvalues, has been derived. This was, unfortunately, not well recognized in the BEM community until Tavara, Ortiz, Mantic and Paris (2008) and Shiah, Tan and Lee (2008) formulated the expressions into computational algorithms for implementation in the BEM, for the special case of transverse isotropy and general anisotropy, respectively. Lee (2003, 2009) further showed how its derivatives could be obtained, although the complete explicit expressions for them in general anisotropy were derived and presented only by the present authors [Shiah, Tan and Lee (2008, 2010)]. These formulations have also been implemented by Tan, Shiah and Lin (2009), and by Buroni and Saez (2010), to analyse some benchmark problems by the BEM.

The Green's function of Ting and Lee (1997) may be expressed in spherical coordinates wherein the spherical angles are periodic. Recognising this, the present

authors have very recently proposed that this Green's function be represented by a simple, double-Fourier series [Shiah, Tan and Wang (2012a,b)]. This approach significantly reduces the computational effort to evaluate the Green's function particularly when there are a large number of field points, as is typically the case for practical problems. It also makes differentiations of the Green's function a straightforward task, resulting in relatively more concise formulations for the derivatives. The major advantage of this scheme is that evaluations of the coefficients for the Fourier series need to be performed only once, regardless of the number of field points involved in the BEM analysis. This makes it very efficient without sacrificing any significant loss of accuracy. To further enhance the computational efficiency, the authors [Tan, Shiah and Wang (2013)] reformulated the expressions by rearranging and simplifying the terms where possible, and eliminated repeated calculations. As a result, the number of terms in the Fourier series is reduced by more than half.

In the direct formulation of the BIE, it is well known that when thermal effects and/or body forces are included, they are manifested by the presence of an extra domain integral. Direct evaluation of this integral requiring domain discretization will destroy the notion of the BEM as a boundary solution technique. Several different schemes, first developed for treating these problems in isotropic elasticity, have been proposed to transform the volume/domain integral into surface/boundary integrals. They include the dual reciprocity method [e.g., Partridge, Brebbia and Wrobel (1994), Schclar (1994), Kogl and Gaul (2003)], particular integral approach [e.g., Deb and Banerjee (1990), Deb, Henry and Wilson (1992)], and the exact transformation method (ETM) [e.g., Rizzo and Shippy (1979), Tan (1983), Danson (1983)]. The first two of these schemes are approximate analytical schemes. The ETM, on the other hand, is analytically exact and can be applied to problems involving geometric singularities, such as those with cracks and re-entrant corners, without re-formulation. It is thus the most attractive approach among them. For anisotropic elasticity, however, the ETM has, to the authors' knowledge, been successfully implemented only in 2D [Zhang, Tan and Afagh (1996), Shiah and Tan (1999a,b; 2000)]; the exact, analytical volume-to-surface integral transformation in this approach for 3D has, hitherto, remained elusive due to the complexity of the Green's function and its derivatives.

Although the fundamental solution presented by Ting and Lee (1997) is fully explicit in terms of the Stroh eigenvalues, the latter need to be determined numerically, thereby posing a potential hurdle to the task of the volume-to-surface integral transformation. For the much simpler case of transversely isotropy, the authors [Shiah and Tan (2012b)] have achieved this end, but some of the kernels of the transformed surface integrals were not explicitly derived into algebraic forms; they

are, instead, numerically determined. In the course of the work, the authors found that the Fourier-series representation of the Green's function is a suitable form to facilitate the transformation. In the integral transformation process, the volume integral is first redefined in a mapped domain, where the thermal field is governed by a standard Laplace equation. The aim of the present study is to extend this to general 3D anisotropy and it follows a similar vein. This will now be described and discussed below. It will be followed by some numerical examples to demonstrate the success of the volume-to-surface integral transformation. Before all these, however, it is useful, first, to provide a brief review of the integral equation for the BEM in thermoelasticity and the Fourier representation of the Green's function of Ting and Lee (1997) as developed by the authors in Tan, Shiah and Wang (2013).

2 Integral equation of 3D anisotropic thermoelasticity

It is well known that in elastic stress analysis, thermal effects can be represented by a pseudo- or equivalent body force term in the governing equations. In the basic direct formulation of the BEM, the integral equation relating the nodal displacements u_j and tractions t_j on the surface S of the homogeneous elastic domain when body-forces or their equivalence, X_i, are present, can be expressed in indicial notation as

$$C_{ij}(P)\,u_i(P)+\int_s u_i(Q)\,\mathrm{T}_{ij}(P,Q)dS(Q)=\int_s t_i(Q)\,\mathrm{U}_{ij}(P,Q)dS(Q)+\int_\Omega X_i\,\mathrm{U}_{ij}(P,q)d\Omega(q) \tag{1}$$

In Equation (1), $U_{ij}(P,Q)\equiv\mathbf{U(x)}$ and $T_{ij}(P,Q)$ represent the fundamental solution of displacements and tractions, respectively, and $C_{ij}(P)$ depends on the geometry at the source point P on boundary. This equation is not truly a BIE as the last term is a volume integral over the domain $\Omega(q)$, where q is an arbitrary field point. To restore this equation into a BIE, this volume integral term has to be transformed into surface integrals. This is the primary focus of the present study.

An explicit form of $\mathbf{U(x)} = U_{ij}$ has been derived by Ting and Lee (1997) and it is expressed as follows,

$$\mathbf{U}(\mathbf{x})=\frac{1}{4\pi r}\frac{1}{|\boldsymbol{\kappa}|}\sum_{\mathrm{n}=0}^{4} q_n\hat{\mathbf{\Gamma}}^{(\mathrm{n})}, \tag{2}$$

where r represents the radial distance between the source and field points; and the

quantities q_n, $\hat{\mathbf{\Gamma}}^{(\mathrm{n})}$, and $\boldsymbol{\kappa}$ are given by

$$\mathrm{q_n}=\begin{cases} \frac{-1}{2\beta_1\beta_2\beta_3}\left[\mathrm{Re}\left\{\sum\limits_{\mathrm{t}=1}^{3}\frac{\mathrm{p_t^n}}{(\mathrm{p_t}-\bar{\mathrm{p}}_{\mathrm{t}+1})(\mathrm{p_t}-\bar{\mathrm{p}}_{\mathrm{t}+2})}\right\}-\delta_{\mathrm{n}2}\right] for \mathrm{n}=0,1,2, \\ \frac{1}{2\beta_1\beta_2\beta_3}\mathrm{Re}\left\{\sum\limits_{\mathrm{t}=1}^{3}\frac{\mathrm{p_t^{n-2}}\bar{\mathrm{p}}_{\mathrm{t}+1}\bar{\mathrm{p}}_{\mathrm{t}+2}}{(\mathrm{p_t}-\bar{\mathrm{p}}_{\mathrm{t}+1})(\mathrm{p_t}-\bar{\mathrm{p}}_{\mathrm{t}+2})}\right\} for \mathrm{n}=3,\ 4, \end{cases} \tag{3a}$$

$$\hat{\Gamma}^{(\mathrm{n})}_{\mathrm{ij}}=\tilde{\Gamma}^{(\mathrm{n})}_{(i+1)(j+1)(i+2)(j+2)}-\tilde{\Gamma}^{(\mathrm{n})}_{(i+1)(j+2)(i+2)(j+1)},\quad (\mathrm{i,j}=1,\ 2,\ 3), \tag{3b}$$

$$\boldsymbol{\kappa}_{\mathrm{ik}}=\mathrm{C_{ijks}m_j m_s},\quad \mathbf{m}=(-\sin\theta,\ \cos\theta,\ 0) \tag{3c}$$

In Equation (3c), the spherical angle θ is as defined in Figure 1, and C_{ijks} are the stiffness coefficients of the material. In Equation (3a), the quantity, p_i, denotes the Stroh eigenvalues and they appear as three pairs of complex conjugates. They are expressed as

$$\mathrm{p_v}=\alpha_\mathrm{v}+\mathrm{i}\beta_\mathrm{v},\beta_\mathrm{v}>0,(\nu=1,2,3) \tag{4}$$

where the overbar on them denotes the corresponding conjugate.

In terms of the spherical coordinates as shown in Figure 1, the Green's function can be re-expressed as

$$\mathbf{U}(r,\theta,\phi)=\frac{\mathbf{H}(\theta,\phi)}{4\pi r}, \tag{5}$$

where $\mathbf{H}(\theta,\phi)$, referred to as the Barnett-Lothe tensor, only depends on the spherical angles (θ,ϕ). For the numerical evaluation of the Bartnett-Lothe tensor, Shiah, Tan and Wang (2012), Tan, Shiah and Wang (2013) very recently proposed that it be represented by a double Fourier-series, taking advantage of the periodic nature of the spherical angles. This has been demonstrated to be simpler to implement into a BEM code as well as significantly more efficient in computations.

The double Fourier series representation of this tensor is as follows:

$$H_{uv}(\theta,\phi)=\sum_{m=-a}^{a}\sum_{n=-a}^{a}\lambda_{uv}^{(m,n)}\,e^{\mathrm{i}(m\theta+n\phi)},\quad (u,\ v=1,\ 2,\ 3), \tag{6}$$

where a is an integer sufficiently large to ensure convergence of the series; $\lambda_{uv}^{(m,n)}$ are unknown coefficients are determined by

$$\lambda_{uv}^{(m,n)}=\frac{1}{4\pi^2}\int_{-\pi}^{\pi}\int_{-\pi}^{\pi}H_{uv}(\theta,\phi)\,e^{-\mathrm{i}(m\theta+n\phi)}d\theta\,d\phi. \tag{7}$$

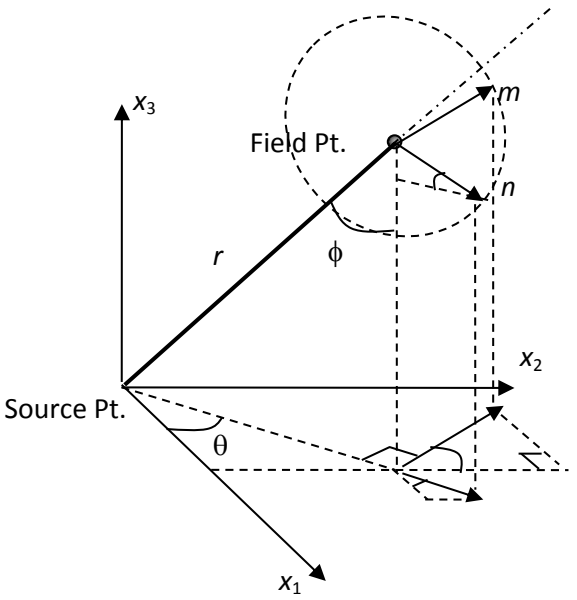

Figure 1: Unit circle on an arbitrary plane at the field point.

The integrals in Equation (7) can be numerically evaluated by, for example, simple Gaussian quadrature, as follows:

$$\lambda_{uv}^{(m,n)} = \frac{1}{4}\sum_{p=1}^{k}\sum_{q=1}^{k} w_p w_q f_{uv}^{(m,n)}(\pi\xi_p, \pi\xi_q), \tag{8}$$

where k is the number of the Gauss abscissa ξ_p, and w_p is the corresponding weight; and $f_{uv}^{(m,n)}(\theta, \phi)$ represents the integrand in Equation (7). Each computation of $\lambda_{uv}^{(m,n)}$ requires the evaluation of $H_{uv}(\theta,\phi)$ at points $(\pi\xi_p, \pi\xi_q)$ using Equations (2)-(4). For large values of m and n, rapid fluctuations of $f_{uv}^{(m,n)}(\theta, \phi)$ may make it necessary to use a relatively large number of Gauss points to accurately perform the numerical integrations. Numerical experiments have shown that with k=64, very accurate integrations for convergent $\mathbf{H}(\theta,\phi)$ have been achieved even for highly anisotropic materials. Of significance to note is that the computation of the Fourier coefficients by Eq.(8) is carried out only once irrespective of the number of field points in the BEM stress analysis. The CPU-time for this process is thus relatively trivial indeed in a BEM analysis of a practical problem.

The 1st-order derivatives of **U**, denoted by **U'**, can be determined from

$$\mathbf{U}' \equiv U_{uv,l} = \frac{\partial U_{uv}}{\partial r}\frac{\partial r}{\partial x_l} + \frac{\partial U_{uv}}{\partial \theta}\frac{\partial \theta}{\partial x_l} + \frac{\partial U_{uv}}{\partial \phi}\frac{\partial \phi}{\partial x_l}. \tag{9}$$

By performing the indicated differentiations, they may be readily shown to have the following Fourier-series forms [Tan, Shiah and Wang (2013)]:

$$U_{uv,l} = \frac{1}{4\pi r^2}\begin{cases} \sum_{m=-a}^{a}\sum_{n=-a}^{a} \lambda_{uv}^{(m,n)} e^{i(m\theta+n\phi)} \begin{bmatrix} -\cos\theta\ (\sin\phi - in\ \cos\phi) \\ -im\ \sin\theta/\sin\phi \end{bmatrix} & \text{for } l=1 \\ \sum_{m=-a}^{a}\sum_{n=-a}^{a} \lambda_{uv}^{(m,n)} e^{i(m\theta+n\phi)} \begin{bmatrix} -\sin\theta\ (\sin\phi - \ in\ \cos\phi) \\ +im\ \cos\theta/\sin\phi \end{bmatrix} & \text{for } l=2 \\ \sum_{m=-a}^{a}\sum_{n=-a}^{a} \lambda_{uv}^{(m,n)} e^{i(m\theta+n\phi)} \left[-(\cos\phi + i\,n\ \sin\phi)\right] & \text{for } l=3 \end{cases} \tag{10}$$

As explained in the above cited reference, the singularity issue at $\phi = 0$ or π in Eq.(10) may be resolved by a simple coordinate transformation; no further discussion need be provided here. The process of volume-to-surface integral transformation will now be discussed.

3 Volume-to-surface integral transformation

As is well known in solid mechanics, thermal effects can be treated as an equivalent body-force in the governing equations in elasticity. It can be easily established that Equation (1) becomes as follows [see, e.g., Rizzo and Shippy (1977)]:

$$\begin{aligned} &C_{ij}(P)\,u_i(P) + \int_s u_i(Q)\,\mathrm{T}_{ij}(P,Q)dS(Q) \\ &= \int_s t_i(Q)\,\mathrm{U}_{ij}(P,Q)dS(Q) + \int_s \gamma_{ik}n_k(Q)\Theta(Q)\ \mathrm{U}_{ij}(P,Q)dS(Q) \\ &- \int_\Omega \gamma_{ik}\Theta_{,k}(Q)\ \mathrm{U}_{ij}(P,q)\ d\Omega \end{aligned} \tag{11}$$

On the right hand side in Equation (11), the last integral is a domain integral that remains to be transformed. For simplicity, this domain integral is denoted by V_j, namely

$$V_j = -\int_\Omega \gamma_{ik}\Theta_{,k}(q)\ U_{ij}(P,q)\,d\Omega, \tag{12}$$

where in anisotropy γ_{ik} are the thermal moduli; Θ stands for the temperature change in anisotropic solid. Following the similar treatment as in Shiah and Tan (1999),

the volume integral in Equation (12) can be redefined in a transformed coordinate system such that the temperature field is governed by the standard Laplace equation, i.e.

$$\Theta_{,\underline{kk}} = 0, \tag{13}$$

where the underline denotes the transformed coordinates. As shown by Shiah and Tan (2004), the transformation of the corresponding governing equation for field problems in general anisotropy in three dimensions (namely, Euler's equation) to Equation (13) can be achieved simply by the following coordinate transformation:

$$\hat{\mathbf{x}}^{\mathbf{T}} = \mathbf{F}\,\mathbf{x}^{\mathbf{T}}. \tag{14}$$

In Equation (14), the transformation matrix $\mathbf{F}$ is given by

$$\mathbf{F} = \begin{pmatrix} \sqrt{\Delta}/K_{11} & 0 & 0 \\ -K_{12}/K_{11} & 1 & 0 \\ \alpha & \beta & \chi \end{pmatrix}, \tag{15}$$

where K_{ij} are the thermal conductivity coefficients; the other coefficients Δ, α, β, and χ are defined by

$$\Delta = K_{11}K_{22} - K_{12}^2, \tag{16a}$$

$$\alpha = (K_{12}K_{23} - K_{13}K_{22})/\sqrt{\omega}, \tag{16b}$$

$$\beta = (K_{12}K_{13} - K_{23}K_{11})/\sqrt{\omega}, \tag{16c}$$

$$\chi = \Delta/\sqrt{\omega}, \tag{16d}$$

$$\omega = K_{11}K_{13}\Delta - K_{11}K_{12}K_{13}^2 + K_{11}K_{12}K_{13}K_{23} - K_{23}^2K_{11}^2. \tag{16e}$$

With this coordinate transformation, the volume integral in Equation (12) can be rewritten as

$$V_j = -\int_{\underline{\Omega}} Z_{\underline{ik}}\Theta_{,\underline{k}}(q)\, U_{\underline{ij}}(P,q)\, d\underline{\Omega}, \tag{17}$$

where $Z_{\underline{ik}}$ are defined by

$$Z_{\underline{ik}} = K_{11}\sqrt{\frac{\omega}{\Delta^3}} \begin{pmatrix} \gamma_{11} & \gamma_{12} & \gamma_{13} \\ \gamma_{21} & \gamma_{22} & \gamma_{23} \\ \gamma_{31} & \gamma_{32} & \gamma_{33} \end{pmatrix} \begin{pmatrix} \sqrt{\Delta}/K_{11} & -K_{12}/K_{11} & \alpha \\ 0 & 1 & \beta \\ 0 & 0 & \chi \end{pmatrix}. \tag{18}$$

Following exactly the same treatment as in Shiah and Tan (1999), V_j can be written in terms of the transformed boundary integrals as follows:

$$V_j = \int_{\underline{S}} Z_{\underline{ik}} \left[\left(\Theta \, W_{\underline{ijk},\underline{t}} - W_{\underline{ijk}} \Theta_{,\underline{t}} \right) n_{\underline{t}} - \Theta \, U_{\underline{ij}} n_{\underline{k}} \right] d\underline{S}, \tag{19}$$

where $W_{\underline{ijk}}$ is a new kernel function which satisfies

$$W_{\underline{ijk},tt} = U_{\underline{ij},k}. \tag{20}$$

The exact analytical volume-to-surface integral transformation is not complete yet unless the very explicit expression of the new function $W_{\underline{ijk}}$ is determined. Herein lies the difficulty in deriving the analytically explicit form of $U_{\underline{ij,k}}$

It should be reminded that the Green's function, $U_{\underline{ij}}$, and its derivatives, $U_{\underline{ij,k}}$, are both defined in the mapped domain. The former can also be written is the transformed spherical coordinate system $(\hat{r}, \hat{\theta}, \hat{\phi})$ as

$$\hat{\mathbf{U}}(\hat{r}, \hat{\theta}, \hat{\phi}) = \frac{\hat{\mathbf{H}}(\hat{\theta}, \hat{\phi})}{4\pi\hat{r}} \tag{21}$$

Similarly, the Fourier series representation of $\hat{\mathbf{H}}(\hat{\theta}, \hat{\phi})$ is given by

$$\hat{H}_{\underline{uv}}(\hat{\theta}, \hat{\phi}) = \sum_{m=-\alpha}^{\alpha} \sum_{n=-\alpha}^{\alpha} \hat{\lambda}_{\underline{uv}}^{(m,n)} \, e^{\mathrm{i}\left(m\hat{\theta} + n\hat{\phi}\right)}, \quad (u, \, v = 1, \, 2, \, 3) \tag{22}$$

where the series coefficients are determined by

$$\hat{\lambda}_{\underline{uv}}^{(m,n)} = \frac{1}{4\pi^2} \int_{-\pi}^{\pi} \int_{-\pi}^{\pi} \hat{H}_{\underline{uv}}(\hat{\theta}, \hat{\phi}) \, e^{-\mathrm{i}\left(m\hat{\theta} + n\hat{\phi}\right)} d\hat{\theta} \, d\hat{\phi}. \tag{23}$$

It is evident that $\hat{H}_{\underline{uv}}(\hat{\theta}, \hat{\phi})$ can be determined using the $\hat{\mathbf{U}}(\hat{x}_1, \hat{x}_2, \hat{x}_3)$, defined in the Cartesian coordinate system for the mapped domain, as follows:

$$\hat{\mathbf{H}}(\hat{\theta}, \hat{\phi}) = 4\pi \, \hat{\mathbf{U}}(\sin\hat{\phi}\cos\hat{\theta}, \sin\hat{\phi}\sin\hat{\theta}, \cos\hat{\phi}) \tag{24}$$

From the coordinate transformation in Equation (14), Equation (24) can be rewritten as

$$\hat{\mathbf{H}}(\hat{\theta}, \hat{\phi}) = 4\pi \mathbf{U}(x_1', x_2', x_3'), \tag{25}$$

where

$$\begin{aligned} x_1' &= \frac{\sqrt{\Delta}}{K_{11}} \sin\hat{\phi}\cos\hat{\theta}, \\ x_2' &= \frac{-K_{12}}{K_{11}} \sin\hat{\phi}\cos\hat{\theta} + \sin\hat{\phi}\sin\hat{\theta}, \\ x_3' &= \alpha \sin\hat{\phi}\cos\hat{\theta} + \beta \sin\hat{\phi}\sin\hat{\theta} + \chi\cos\hat{\phi}. \end{aligned} \tag{26}$$

Thus, Equation (23) is re-expressed as

$$\hat{\lambda}_{\underline{uv}}^{(m,n)} = \frac{1}{4\pi^2}\int_{-\pi}^{\pi}\int_{-\pi}^{\pi}\frac{H_{uv}(\theta',\phi')}{r'}\, e^{-\mathrm{i}\left(m\hat{\theta}+n\hat{\phi}\right)} d\hat{\theta}\, d\hat{\phi}. \tag{27}$$

In Equation (27), (r',θ',ϕ') are all intrinsic functions of $(\hat{\theta},\hat{\phi})$, defined by

$$r' = \sqrt{\left(x_1'\right)^2 + \left(x_2'\right)^2 + \left(x_3'\right)^2}, \quad \theta' = \tan^{-1}\left(\frac{x_2'}{x_1'}\right), \quad \phi' = \cos^{-1}\left(\frac{x_3'}{r'}\right). \tag{28}$$

As a result, $\hat{\lambda}_{\underline{uv}}^{(m,n)}$ can be numerically computed using, for example, Gaussian quadrature, viz

$$\hat{\lambda}_{\underline{uv}}^{(m,n)} = \frac{1}{4}\sum_{p=1}^{k}\sum_{q=1}^{k} w_p w_q \hat{f}_{uv}^{(m,n)}\left(\pi\,\xi_p,\, \pi\,\xi_q\right), \tag{29}$$

where $\hat{f}_{uv}^{(m,n)}(\hat{\theta},\,\hat{\phi})$ is the integrand in Equation (29), i.e.

$$\hat{f}_{uv}^{(m,n)}(\hat{\theta},\,\hat{\phi}) = \frac{H_{uv}(\theta',\phi')}{r'}\, e^{-\mathrm{i}\left(m\hat{\theta}+n\hat{\phi}\right)}. \tag{30}$$

In Equation (30), $H_{uv}(\theta',\phi')$ is directly computed from Equation (6). With all the coefficients, $\hat{\lambda}_{\underline{uv}}^{(m,n)}$, computed via the steps outlined above, the fundamental displacements in the transformed coordinate system can be calculated using the Fourier-series

$$U_{\underline{uv}} = \frac{1}{4\pi\hat{r}}\sum_{m=-a}^{a}\sum_{n=-a}^{a}\hat{\lambda}_{\underline{uv}}^{(m,n)}\, e^{\mathrm{i}\left(m\hat{\theta}+n\hat{\phi}\right)}, \quad (u,\, v = 1,\, 2,\, 3) \tag{31}$$

Similar to Equation (10), the 1st-order derivatives of the fundamental displacements are given by

$$U_{\underline{uv},l} = \frac{1}{4\pi\hat{r}^2}\begin{cases} \sum_{m=-\alpha}^{\alpha}\sum_{n=-\alpha}^{\alpha}\hat{\lambda}_{\underline{uv}}^{(m,n)} e^{i\left(m\hat{\theta}+n\hat{\phi}\right)}\begin{bmatrix} -\cos\hat{\theta}\,\left(\sin\hat{\phi} - in\,\cos\hat{\phi}\right) \\ -im\,\sin\hat{\theta}/\sin\hat{\phi} \end{bmatrix} & \text{for } l=1 \\ \sum_{m=-a}^{a}\sum_{n=-a}^{a}\hat{\lambda}_{\underline{uv}}^{(m,n)} e^{i\left(m\hat{\theta}+n\hat{\phi}\right)}\begin{bmatrix} -\sin\hat{\theta}\,\left(\sin\hat{\phi} - in\,\cos\hat{\phi}\right) \\ +im\,\cos\hat{\theta}/\sin\hat{\phi} \end{bmatrix} & \text{for } l=2 \\ \sum_{m=-a}^{a}\sum_{n=-a}^{a}\hat{\lambda}_{\underline{uv}}^{(m,n)} e^{i\left(m\hat{\theta}+n\hat{\phi}\right)}\left[-\left(\cos\hat{\phi} + i\,n\,\sin\hat{\phi}\right)\right] & \text{for } l=3 \end{cases} \tag{32}$$

Returning now to Equation (20) that is used to define the new third order tensor, $W_{\underline{ijk}}$. In the spherical coordinate system for the mapped domain, Equation (20) can be expressed as

$$\frac{\partial^2 W_{\underline{ijk}}}{\partial\hat{\mathrm{r}}^2} + \frac{2}{\hat{\mathrm{r}}}\frac{\partial W_{\underline{ijk}}}{\partial\hat{\mathrm{r}}} + \frac{1}{\hat{\mathrm{r}}^2}\frac{\partial^2 W_{\underline{ijk}}}{\partial\hat{\phi}^2} + \frac{\cot\hat{\phi}}{\hat{\mathrm{r}}^2}\frac{\partial W_{\underline{ijk}}}{\partial\hat{\phi}} + \frac{1}{\hat{\mathrm{r}}^2\sin^2\hat{\phi}}\frac{\partial^2 W_{\underline{ijk}}}{\partial\hat{\theta}^2} = \frac{\kappa_{\underline{ijk}}(\hat{\theta},\hat{\phi})}{\hat{\mathrm{r}}^2} \tag{33}$$

where

$$\kappa_{\underline{ijk}}(\hat{\theta},\hat{\phi})=\frac{1}{4\pi}\begin{cases}\sum_{m=-a}^{a}\sum_{n=-a}^{a}\hat{\lambda}_{\underline{ij}}^{(m,n)}e^{i(m\hat{\theta}+n\hat{\phi})}\begin{bmatrix}-\cos\hat{\theta}\left(\sin\hat{\phi}-in\cos\hat{\phi}\right)\\-im\ \sin\hat{\theta}/\sin\hat{\phi}\end{bmatrix} & for\ k=1\\ \sum_{m=-a}^{a}\sum_{n=-a}^{a}\hat{\lambda}_{\underline{ij}}^{(m,n)}e^{i(m\hat{\theta}+n\hat{\phi})}\begin{bmatrix}-\sin\hat{\theta}\left(\sin\hat{\phi}-in\cos\hat{\phi}\right)\\+im\ \cos\hat{\theta}/\sin\hat{\phi}\end{bmatrix} & for\ k=2\\ \sum_{m=-a}^{a}\sum_{n=-a}^{a}\hat{\lambda}_{\underline{ij}}^{(m,n)}e^{i(m\hat{\theta}+n\hat{\phi})}\left[-\left(\cos\hat{\phi}+in\sin\hat{\phi}\right)\right] & for\ k=3\end{cases} \tag{34}$$

The satisfaction of Equation (33) implies that $W_{\underline{ijk}}$ depends only on the spherical angles but not the radial coordinate. For this reason, it is written simply as $W_{\underline{ijk}}(\hat{\theta},\hat{\phi})$ and Equation (33) is simplified into

$$\frac{\partial^2 W_{\underline{ijk}}(\hat{\theta},\hat{\phi})}{\partial\hat{\phi}^2}+\cot\hat{\phi}\frac{\partial W_{\underline{ijk}}(\hat{\theta},\hat{\phi})}{\partial\hat{\phi}}+\frac{1}{\sin^2\hat{\phi}}\frac{\partial^2 W_{\underline{ijk}}(\hat{\theta},\hat{\phi})}{\partial\hat{\theta}^2}=\kappa_{\underline{ijk}}(\hat{\theta},\hat{\phi}). \tag{35}$$

Under the general condition when $\hat{\phi}\neq 0$ or π, Equation (35) can be further rewritten as

$$\sin^2\hat{\phi}\frac{\partial^2 W_{\underline{ijk}}(\hat{\theta},\hat{\phi})}{\partial\hat{\phi}^2}+\frac{\sin 2\hat{\phi}}{2}\frac{\partial W_{\underline{ijk}}(\hat{\theta},\hat{\phi})}{\partial\hat{\phi}}+\frac{\partial^2 W_{\underline{ijk}}(\hat{\theta},\hat{\phi})}{\partial\hat{\theta}^2}=\kappa_{\underline{ijk}}(\hat{\theta},\hat{\phi})\sin^2\hat{\phi}. \tag{36}$$

By taking advantage of the periodical nature of the spherical angles, $W_{\underline{ijk}}(\hat{\theta},\hat{\phi})$ can be expressed as a Fourier series,

$$W_{\underline{ijk}}(\hat{\theta},\hat{\phi})=\sum_{m=-a}^{a}\sum_{n=-a}^{a}\tilde{C}_{\underline{ijk}}^{(m,n)}e^{i(m\hat{\theta}+n\hat{\phi})}, \tag{37}$$

where $\tilde{C}_{\underline{ijk}}^{(m,n)}$ are unknown coefficients to be determined. Substituting Equation (37) directly into Equation (36) yields

$$\frac{-1}{2}\sum_{m=-a}^{a}\sum_{n=-a}^{a}\tilde{C}_{\underline{ijk}}^{(m,n)}\left(n^2+2m^2-n^2\cos 2\hat{\phi}-in\sin 2\hat{\phi}\right)e^{i(m\hat{\theta}+n\hat{\phi})}=\kappa_{\underline{ijk}}(\hat{\theta},\hat{\phi})\sin^2\hat{\phi} \tag{38}$$

For determining the unknown coefficients, both sides of Equation (38) are integrated as follows:

$$\begin{aligned}&\tfrac{-1}{2\pi^2}\int_{-\pi}^{\pi}\int_{-\pi}^{\pi}\sum_{m=-a}^{a}\sum_{n=-a}^{a}\tilde{C}_{\underline{ijk}}^{(m,n)}\left(n^2+2m^2-n^2\cos 2\hat{\phi}-in\sin 2\hat{\phi}\right)e^{i(m\hat{\theta}+n\hat{\phi})}e^{-i(p\hat{\theta}+q\hat{\phi})}d\hat{\theta}d\hat{\phi}\\&=\tfrac{1}{\pi^2}\int_{-\pi}^{\pi}\int_{-\pi}^{\pi}\kappa_{\underline{ijk}}(\hat{\theta},\hat{\phi})\sin^2\hat{\phi}\;e^{-i(p\hat{\theta}+q\hat{\phi})}d\hat{\theta}\;d\hat{\phi}\end{aligned}\quad . \tag{39}$$

From the orthogonality relationships of the trigonometric functions, the above integrations of the left hand side (LHS) and right hand side (RHS) of Equation (39) yield the following nonzero values:

$$\text{LHS: } \tilde{C}_{\underline{ijk}}^{(m,n)}\begin{cases}-2(2m^2+n^2) & (\text{for } m=p\,,\,n=q)\\ n(n-1) & (\text{for } m=p\,,\,n=q+2)\\ n(n+1) & (\text{for } m=p\,,\,n=q-2)\end{cases}, \tag{40a}$$

$$\text{RHS (when } k\text{=1): }\frac{i\hat{\lambda}_{\underline{ij}}^{(m,n)}}{4}\begin{cases}(4m+n-3) & (\text{for } m=p+1\,,\,n=q+1)\\ -(n-1) & (\text{for } m=p+1\,,\,n=q+3)\\ -(4m-n-3) & (\text{for } m=p+1\,,\,n=q-1)\\ -(n+1) & (\text{for } m=p+1\,,\,n=q-3)\\ (-4m+n-3) & (\text{for } m=p-1\,,\,n=q+1)\\ -(n-1) & (\text{for } m=p-1\,,\,n=q+3)\\ (4m+n-3) & (\text{for } m=p-1\,,\,n=q-1)\\ -(n+1) & (\text{for } m=p-1\,,\,n=q-3)\end{cases}, \tag{40b}$$

$$\text{RHS (when } k\text{=2): }\frac{i\hat{\lambda}_{\underline{ij}}^{(m,n)}}{4}\begin{cases}-(4m+n-3) & (\text{for } m=p+1\,,\,n=q+1)\\ (n-1) & (\text{for } m=p+1\,,\,n=q+3)\\ (4m-n-3) & (\text{for } m=p+1\,,\,n=q-1)\\ (n+1) & (\text{for } m=p+1\,,\,n=q-3)\\ (-4m+n-3) & (\text{for } m=p-1\,,\,n=q+1)\\ -(n-1) & (\text{for } m=p-1\,,\,n=q+3)\\ (4m+n-3) & (\text{for } m=p-1\,,\,n=q-1)\\ -(n+1) & (\text{for } m=p-1\,,\,n=q-3)\end{cases}, \tag{40c}$$

$$\text{RHS (when } k\text{=3): }\frac{i\hat{\lambda}_{\underline{ij}}^{(m,n)}}{4}\begin{cases}(3n-1) & (\text{for } m=p\,,\,n=q+1)\\ -(n-1) & (\text{for } m=p\,,\,n=q+3)\\ -(3n+1) & (\text{for } m=p\,,\,n=q-1)\\ (n+1) & (\text{for } m=p\,,\,n=q-3)\end{cases}. \tag{40d}$$

These integrations for all values of p, q ranging from -a to +a result in a system of equations, expressed in the following banded matrix form:

$$\begin{bmatrix} M_1 & 0 & \widehat{M}_1 & 0 & 0 & \cdots & 0 & 0 & 0 & 0 & 0 \\ 0 & M_2 & 0 & \widehat{M}_2 & 0 & \cdots & 0 & 0 & 0 & 0 & 0 \\ \breve{M}_3 & 0 & M_3 & 0 & \widehat{M}_3 & \cdots & 0 & 0 & 0 & 0 & 0 \\ 0 & \breve{M}_4 & 0 & M_4 & 0 & \cdots & 0 & 0 & 0 & 0 & 0 \\ 0 & 0 & \breve{M}_5 & 0 & M_5 & \cdots & 0 & 0 & 0 & 0 & 0 \\ \vdots & \vdots & \vdots & \vdots & \vdots & \ddots & \vdots & \vdots & \vdots & \vdots & \vdots \\ 0 & 0 & 0 & 0 & 0 & \cdots & M_{t-4} & 0 & \widehat{M}_{t-4} & 0 & 0 \\ 0 & 0 & 0 & 0 & 0 & \cdots & 0 & M_{t-3} & 0 & \widehat{M}_{t-3} & 0 \\ 0 & 0 & 0 & 0 & 0 & \cdots & \breve{M}_{t-2} & 0 & M_{t-2} & 0 & \widehat{M}_{t-2} \\ 0 & 0 & 0 & 0 & 0 & \cdots & 0 & \breve{M}_{t-1} & 0 & M_{t-1} & 0 \\ 0 & 0 & 0 & 0 & 0 & \cdots & 0 & 0 & \breve{M}_t & 0 & M_t \end{bmatrix} \begin{bmatrix} \bar{C}_{ijk}^{(1)} \\ \bar{C}_{ijk}^{(2)} \\ \bar{C}_{ijk}^{(3)} \\ \bar{C}_{ijk}^{(4)} \\ \bar{C}_{ijk}^{(5)} \\ \vdots \\ \bar{C}_{ijk}^{(t-4)} \\ \bar{C}_{ijk}^{(t-3)} \\ \bar{C}_{ijk}^{(t-2)} \\ \bar{C}_{ijk}^{(t-1)} \\ \bar{C}_{ijk}^{(t)} \end{bmatrix} = \begin{bmatrix} \Upsilon_{ijk}^{(1)} \\ \Upsilon_{ijk}^{(2)} \\ \Upsilon_{ijk}^{(3)} \\ \Upsilon_{ijk}^{(4)} \\ \Upsilon_{ijk}^{(5)} \\ \vdots \\ \Upsilon_{ijk}^{(t-4)} \\ \Upsilon_{ijk}^{(t-3)} \\ \Upsilon_{ijk}^{(t-2)} \\ \Upsilon_{ijk}^{(t-1)} \\ \Upsilon_{ijk}^{(t)} \end{bmatrix} \tag{41}$$

where $\bar{C}_{ijk}^{(u)}$ is used to denote the u-th coefficient of each set of $\tilde{C}_{ijk}^{(m,n)}$, numbered in sequential order; $\Upsilon_{ijk}^{(v)}$ represents the RHS value as defined in Equations (40b)$\sim$(40d) for the v-th equation. In Equation (41), M_u, $\widehat{M}_u$, $\breve{M}_u$ are defined as follows:

$$\begin{aligned} M_u &= -2(2m^2+n^2) \quad (\text{for } m=p\,,\, n=q), \\ \widehat{M}_u &= n(n-1) \qquad\quad (\text{for } m=p\,,\, n=q+2), \\ \breve{M}_u &= n(n+1) \qquad\quad (\text{for } m=p\,,\, n=q-2). \end{aligned} \tag{42}$$

Since $\tilde{C}_{ijk}^{(0,0)}$ is associated with the rigid body motion, its corresponding equation with all zero coefficients should be removed from the system of equations and one may choose the null value for it. Thus, the resulting matrix will be of order $[(2a+1)^2\text{-}1] \times [(2a+1)^2\text{-}1]$. Equation (41) can be solved relatively quickly for the Fourier coefficients due to the banded matrix. It should also be reminded that solving for these coefficients is done only once irrespective of the number of field points involved in the BEM analysis. As for the proper choice of the value of a, extensive numerical experiments have shown that a=22 is a sufficiently large number to ensure very accurate results here. As a further saving in computational effort, one may also pre-calculate and store the inverse of the banded matrix, as the coefficients of

the banded matrix are independent of material properties and the indices With all coefficients determined from Equation (41), the explicit expression for $W_{\underline{ijk}}(\hat{\theta},\hat{\phi})$ is given by Equation (37). By performing partial differentiations in the spherical coordinate system, its first-order derivatives are given by

$$W_{\underline{ijk},t}(\hat{r},\hat{\theta},\hat{\phi})=\frac{1}{\hat{r}}\begin{cases}\sum_{m=-a}^{a}\sum_{n=-a}^{a}\tilde{C}_{\underline{ijk}}^{(m,n)}e^{\mathrm{i}(m\hat{\theta}+n\hat{\phi})}\left(in\cos\hat{\theta}\cos\hat{\phi}-im\sin\hat{\theta}/\sin\hat{\phi}\right) & (\text{for } t=1)\\ \sum_{m=-a}^{a}\sum_{n=-a}^{a}\tilde{C}_{\underline{ijk}}^{(m,n)}e^{\mathrm{i}(m\hat{\theta}+n\hat{\phi})}\left(in\sin\hat{\theta}\cos\hat{\phi}+im\cos\hat{\theta}/\sin\hat{\phi}\right) & (\text{for } t=2)\\ \sum_{m=-a}^{a}\sum_{n=-a}^{a}\tilde{C}_{\underline{ijk}}^{(m,n)}e^{\mathrm{i}(m\hat{\theta}+n\hat{\phi})}\left(-in\sin\hat{\phi}\right) & (\text{for } t=3)\end{cases} \tag{43}$$

Up to this point, the new tensor and its derivatives are well defined in the transformed coordinate system and the transformed boundary integrals in Equation (19) can be computed in the usual manner in BEM analysis.

4 Numerical tests

To demonstrate the veracity of the above volume-to-surface integral transformation for the domain integral associated with thermal loads in BEM, the results of a few numerical tests are presented here. The main focus is to show the equivalence of the original domain integral and the transformed surface ones. For the first test, quartz with the following stiffness coefficients [Nye (1960)] defined in its principal directions, denoted by $\mathbf{C}^*$, is selected as the material:

$$\mathbf{C}^*=\begin{bmatrix}87.6 & 6.07 & 13.3 & 17.3 & 0 & 0\\ 6.07 & 87.6 & 13.3 & -17.3 & 0 & 0\\ 13.3 & 13.3 & 106.8 & 0 & 0 & 0\\ 17.3 & -17.3 & 0 & 57.2 & 0 & 0\\ 0 & 0 & 0 & 0 & 57.2 & 17.3\\ 0 & 0 & 0 & 0 & 17.3 & 40.765\end{bmatrix}\ \text{GPa}. \tag{44}$$

With successive clockwise rotation of the principal axes by 30°, 45° and 60° with respect to the x_1, x_2 and x_3-axis, respectively, the corresponding stiffness coefficients in the global Cartesian coordinate system is obtained which has the features

of a generally anisotropic material:

$$\mathbf{C} = \begin{pmatrix} 111.8489 & 14.8019 & -5.2389 & -0.2525 & 11.0164 & -14.0224 \\ 14.8019 & 101.8225 & -7.5773 & 0.3963 & -0.6162 & 18.8720 \\ -5.2389 & -7.5773 & 129.6975 & 4.3933 & 1.5637 & 0.6272 \\ -0.2525 & 0.3963 & 4.3933 & 31.2929 & 2.5347 & 3.5506 \\ 11.0164 & -0.6162 & 1.5637 & 2.5347 & 37.9378 & 1.3277 \\ -14.0224 & 18.8720 & 0.6272 & 3.5506 & 1.3277 & 55.2450 \end{pmatrix} \text{ GPa} \tag{45}$$

A second material, namely, alumina (Al_2O_3) is also selected as a further check. In its principal directions of the material properties, it has the following stiffness coefficients [Nye (1960)]:

$$\mathbf{C}^* = \begin{bmatrix} 465 & 124 & 117 & 0 & 0 & 0 \\ 124 & 465 & 117 & 0 & 0 & 0 \\ 117 & 117 & 563 & 0 & 0 & 0 \\ 0 & 0 & 0 & 233 & 0 & 0 \\ 0 & 0 & 0 & 0 & 233 & 0 \\ 0 & 0 & 0 & 0 & 0 & 170.5 \end{bmatrix} \text{ GPa.} \tag{46}$$

Successive counterclockwise rotation of the principal axes about the x_1-, x_2- and x_3-axis by 20°, 80° and 150°, respectively, yields the following stiffness matrix with respect to the global Cartesian system:

$$\mathbf{C} = \begin{pmatrix} 564.7664 & 113.5682 & 113.7194 & -3.7359 & -1.9834 & -2.0239 \\ 113.5682 & 471.4372 & 123.5177 & 3.1022 & -1.7179 & 18.4872 \\ 113.7194 & 123.5177 & 471.1860 & 3.1063 & 18.1411 & -1.7284 \\ -3.7359 & 3.1022 & 3.1063 & 173.7951 & 9.5251 & 9.3103 \\ -1.9834 & -1.7179 & 18.1411 & 9.5251 & 227.7924 & -1.8476 \\ -2.0239 & 18.4872 & -1.7284 & 9.3103 & -1.8486 & 227.7177 \end{pmatrix} \text{ GPa.} \tag{47}$$

Using a=22 in the procedure as explained above, the coefficients of $W_{\underline{ijk}}(\hat{\theta}, \hat{\phi})$ were computed. The satisfaction of Equation (20) at a few sample field points in the mapped domain was checked for all 18 independent sets of $W_{\underline{ijk}}(\hat{\theta}, \hat{\phi})$. For this purpose, the Laplacian operations of $W_{\underline{ijk}}$ were approximated using the central difference scheme, while $U_{ij,k}$ was determined by Equation (32). Since the computations for all 18 independent sets showed similar accuracy, only a typical case for W_{131} was arbitrarily chosen. The numerical results are listed in Table 1. As has been explained in Shiah, Tan and Wang (2012), the singularity when $\hat{\phi}$= 0 or π can

be removed by coordinate redefinition. To further demonstrate this, two sample points along the x_3-axis were also included in the test. As can be seen from the table, the computed W_{131} accurately satisfies Equation (20) for all the sample field points with negligible truncation errors.

The next set of tests is to verify the equivalence of the original volume integral defined in Equation (12) and the transformed surface integrals, given in Equation (19). Figure 2 shows the BEM mesh used to model a cube. For this purpose, the stiffness coefficients in Equation (47) are used; the other thermal material properties (conductivity coefficients $\mathbf{K}$ and thermal expansion coefficients $\boldsymbol{\alpha}$, are assumed as follows:

$$\mathbf{K} = \begin{pmatrix} 21.0104 & -10.1401 & -0.5520 \\ -10.1401 & 24.5785 & 1.6656 \\ -0.5520 & 1.6656 & 23.4811 \end{pmatrix} \; W \cdot m/^0C, \tag{48a}$$

$$\boldsymbol{\alpha} = \begin{pmatrix} 0.2612 & -0.5760 & -0.2129 \\ -0.5760 & 0.2838 & 0.2015 \\ -0.2129 & 0.2015 & 0.1600 \end{pmatrix} \times 10^{-6}/^0C. \tag{48b}$$

With these values, the thermal moduli of the original domain are determined, from the basic theory of thermoelasticity, to be:

$$\boldsymbol{\gamma} = \begin{pmatrix} 0.1981E+02 & -0.2134E+01 & -0.7204E+00 \\ -0.2134E+01 & 0.1813E+02 & 0.5929E+00 \\ -0.7204E+00 & 0.5929E+00 & 0.1397E+02 \end{pmatrix} \times 10^{-5} \; GPa/^0C. \tag{49}$$

From Equation (18), one obtains

$$\boldsymbol{Z} = \begin{pmatrix} 0.2158\text{E}+02 & 0.8360\text{E}+01 & -0.2181\text{E}+01 \\ -0.2325\text{E}+01 & 0.1925\text{E}+02 & 0.6188\text{E}+00 \\ -0.7849\text{E}+00 & 0.2760\text{E}+00 & 0.1448\text{E}+02 \end{pmatrix} \times 10^{-5} \; \text{GPa}/^0C. \tag{50}$$

The following temperature distribution is arbitrarily assumed for this test:

$$\Theta = (0.96794x_1 + 3)(0.4826x_1 + x_2 - 2)(-0.0652x_1 - 0.0074x_2 + 0.9178x_3 + 5) \tag{51}$$

It satisfies the corresponding anisotropic heat conduction equation. Under the transformed coordinate system, the temperature distribution in the mapped domain can be easily verified to be

$$\Theta = (\hat{x}_{\underline{1}} + 3)(\hat{x}_{\underline{2}} - 2)(\hat{x}_{\underline{3}} + 5). \tag{52}$$

Table 1: Comparison between $\nabla^2 W_{\underline{131}}$ and $U_{\underline{13,1}}$ for some sample field points.

Field point coordinate	Quartz		Alumina	
	$\nabla^2 W_{\underline{131}} \times 10^9$	$U_{\underline{13,1}} \times 10^9$	$\nabla^2 W_{\underline{131}} \times 10^9$	$U_{\underline{13,1}} \times 10^9$
(1.25,3.75,6.50)	0.4205E-03 (0.00%)	0.42049E-03	0.7390E-03 (0.00%)	0.7390E-03
(-1.25,3.75,6.50)	0.2429E-03 (0.00%)	0.2429E-03	0.7158E-03 (0.00%)	0.7158E-03
(-1.25,-3.75,6.50)	0.1479E-03 (0.00%)	0.1479E-03	0.7579E-03 (0.00%)	0.7579E-03
(1.25,-3.75,6.50)	0.3632E-03 (0.00%)	0.3632E-03	0.7501E-03 (0.00%)	0.7501E-03
(1.25,3.75,-6.50)	-0.1479E-03 (0.00%)	-0.1479E-03	-0.7579E-03 (0.00%)	-0.7579E-03
(-1.25,3.75,-6.50)	-0.3632E-03 (0.00%)	-0.3632E-03	-0.7501E-03 (0.00%)	-0.7501E-03
(-1.25,-3.75,-6.50)	-0.4205E-03 (0.00%)	-0.4205E-03	-0.7390E-03 (0.00%)	-0.7390E-03
(1.25,-3.75-,6.50)	-0.2429E-03 (0.00%)	-0.2429E-03	-0.7158E-03 (0.00%)	-0.7158E-03
(0.00,0.00,1.00)	0.7074E-01 (0.00%)	0.7074E-01	0.5923E-01 (0.00%)	0.5923E-01
(0.00,0.00,-1.00)	-0.7074E-01 (0.00%)	-0.7074E-01	-0.5923E-01 (0.00%)	-0.5923E-01

As shown in Figure 2, the cube (2 units$\times$2 units$\times$2 units) is modeled with 24 quadratic boundary elements. The eight nodes at the corners are selected as the sample source points. Purely for the purpose to verify the analytical exactness of Equation (19), the volume integral was integrated using a 100-points Gauss quadrature scheme, while over each of the boundary elements, the 8-points Gauss quadrature was employed. Table 2 lists the results of the computations; it can be seen that the percentage deviations of the numerical values of the domain integral and the corresponding transformed surface integrals are very small indeed.

A slightly more complex geometry is considered to further test the validity of the volume-to-surface integral transformation. It is a hollow cylinder as shown in Figure 3, with inner radius of unit, outer radius, 2 units, and height, 2 units. A relatively refined mesh of 96 boundary elements was employed. The material properties were taken to be the same as those used in the previous example. Purely for convenience, the same temperature distribution as given by Equations (51, 52) was also used; this

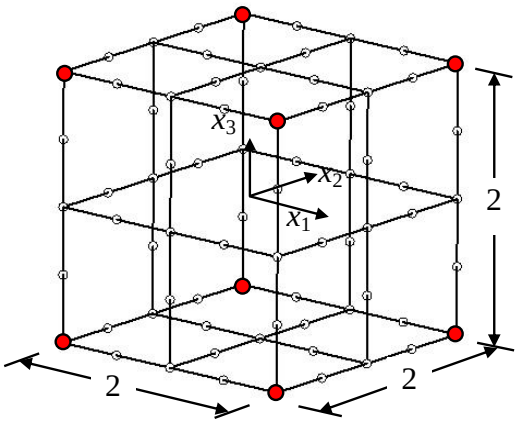

Figure 2: BEM mesh of a cube domain.

Table 2: Comparison of the integrated values of V_j – cube.

Source pt.	V_j computed by Eq.(12)			V_j computed by Eq.(19)		
	j=1	j=2	j=3	j=1	j=2	j=3
(1.0,1.0,1.0)	0.1114E+04	-0.4125E+04	0.8220E+3	0.1119E+04 (0.46%)	-0.4118E+04 (0.17%)	0.8295E+3 (0.92%)
(1.0,-1.0,1.0)	0.1444E+04	-0.4437E+04	0.4994E+03	0.1434E+04 (0.70%)	-0.4426E+04 (0.26%)	0.5079E+3 (171%)
(1.0,1.0,1.0)	0.3774E+3	-0.4434E+04	0.1304E+04	0.3758E+3 (0.44%)	-0.4436E+04 (0.04%)	0.1306E+04 (0.15%)
(-1.0,1.0,1.0)	0.1454E+04	-0.4348E+04	0.1376E+04	0.1457E+04 (0.19%)	-0.4351E+04 (0.08%)	0.1378E+04 (0.16%)
(1.0,1.0,1.0)	0.9778E+3	-0.4411E+04	0.1304E+04	0.9868E+3 (0.92%)	-0.4402E+04 (0.21%)	0.1293E+04 (0.82%)
(1.0,-1.0,1.0)	0.1768E+04	-0.5038E+04	0.1704E+04	0.1753E+04 (0.80%)	-0.5021E+04 (0.33%)	0.1693E+04 (0.65%)
(1.0,1.0,1.0)	0.5238E+3	-0.4646E+04	0.5487E+3	0.5219E+3 (0.38%)	-0.4649E+04 (0.06%)	0.5457E+3 (0.54%)
(-1.0,1.0,1.0)	0.1391E+04	-0.4308E+04	0.4417E+3	0.1396E+04 (0.30%)	-0.4313E+04 (0.131%)	0.4381E+3 (0.80%)

does not detract the validity of the numerical test. As before, the volume integration was performed using 100-points Gauss quadrature, but in the cylindrical coordinate system, as follows,

$$\begin{aligned} V_j &= -\int_{-1}^{1}\int_{0}^{2\pi}\int_{1}^{2} \gamma_{ik}\Theta_{,k}(r,\theta,z)\, U_{ij}(r,\theta,z)\, r dr\, d\theta\, dz \\ &= -\frac{\pi}{2}\sum_{s=1}^{100}\sum_{u=1}^{100}\sum_{v=1}^{100}\left[\begin{array}{l} \gamma_{ik}\Theta_{,k}(0.5\xi_v+1.5,\pi\xi_u+\pi,\xi_s) \\ U_{ij}(0.5\xi_v+1.5,\pi\xi_u+\pi,\xi_s)\ (0.5\xi_v+1.5)\, w_s w_u w_v \end{array}\right] \end{aligned} \tag{53}$$

Similarly, the surface integrals over each of the boundary elements in the BEM mesh were computed with 8-points Gauss quadrature as before. Table 3 lists the computed results of the numerical evaluations of V_j as a domain integral directly and as the corresponding transformed surface integral, respectively. It can be seen again that there is very good agreement between both sets of results. The slightly greater percentage deviations may be attributed to the errors introduced in the numerical modeling of the geometry by the assemblage of discrete boundary elements and in the numerical integrations over them Although not presented here, these small deviations have been verified to decrease further when higher order Gauss quadrature schemes were used for the elements.

The numerical tests above have provided a clear demonstration of the veracity of the exact integral transformation for the domain integral associated with thermal effects in the formulation of the boundary integral equation (BIE) for 3D thermoelastic stress analysis of a generally anisotropic solid It restores the notion of the BEM as a boundary solution technique without the need of making simplifying approximation schemes as it is analytically exact.

5 Conclusions

In conventional BEM for elastic stress analysis, thermal effects give rise to a domain integral in the primary form of the integral equation. Unless it is transformed into surface integrals, this domain integral destroys the notion of the BEM as a boundary solution technique as the integral equation is no longer a true BIE. Among all the schemes developed to treat this issue, the exact transformation approach is perhaps the most elegant from the viewpoint of its analytical exactness Thus, it does not suffer the limitations of approximation methods that have been employed in BEM modeling. This approach has, however, only been successfully applied to isotropic thermoelasticity and in the 2D general anisotropic case Its extension to 3D generally anisotropic thermoelasticity has, hitherto, remained elusive. The major challenge stems from the mathematical complexity of the associated Green's function for 3D generally anisotropic elastic bodies. In this study, the exact volume-to-surface integral transformation of the domain integral associated with thermal

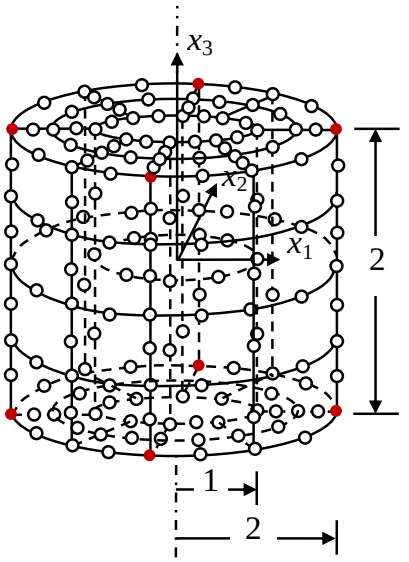

Figure 3: A hollow cylinder for numerical test.

Table 3: Comparison of the integrated values of V_j – hollow cylinder.

Source pt.	V_j computed by Eq.(12)			V_j computed by Eq.(19)		
	j=1	j=2	j=3	j=1	j=2	j=3
(0.0,2.0,-1.0)	0.3006E+04	-0.8734E+04	0.1221E+04	0.3002E+04 (0.13%)	-0.8678E+04 (0.64%)	0.1261E+04 (3.28%)
(2.0,0.0,-1.0)	0.1125E+03	-0.8712E+04	0.1681E+04	0.1102E+03 (2.06%)	-0.8704E+04 (0.09%)	0.1702E+04 (1.21%)
(0.0,2.0,-1.0)	0.1066E+04	-0.8048E+04	0.1792E+04	0.1067E+04 (0.6%)	-08043E+04 (0.07%)	0.1791E+04 (0.04%)
(-2.0,0.0,-1.0)	0.3268E+04	-0.7363E+04	0.1890E+04	0.3281E+04 (0.39%)	-0.7358E+04 (0.07%)	0.1902E+04 (0.64%)
(0.0,2.0,1.0)	0.3153E+04	-0.9603E+04	0.3243E+04	0.3151E+04 (0.07%)	-0.9528E+04 (0.78%)	0.3183E+04 (1.83%)
(2.0,0.0,1.0)	0.1465E+04	-0.9306E+04	0.1840E+04	0.1437E+04 (1.97%)	-0.9298E+04 (0.09%)	0.1812E+04 (1.55%)
(0.0,2.0,1.0)	0.1046E+04	-0.8187E+04	0.4991E+03	0.1047E+04 (0.11%)	-0.8181E+04 (0.07%)	0.4990E+04 (0.01%)
(-2.0,0.0,1.0)	0.3183E+04	-0.7348E+04	0.1140E+04	0.3205E+04 (0.70%)	-0.7343E+04 (0.06%)	0.1119E+04 (1.85%)

effects has been successfully achieved using a Fourier series representation of Ting and Lee's (1997) Green's function as proposed by the authors very recently The transformation follows the same basic steps as carried out by the authors previously in 2D general anisotropy. The anisotropic temperature field is first, mapped into another Cartesian system of coordinates so that the governing equation becomes the simple Laplace equation. The integral transformation is then carried out in this mapped domain. The veracity of the process has been checked by a number of tests where excellent agreement has been obtained from the numerically evaluated values of the domain integral and the corresponding transformed surface integrals. This development will thus restore the BEM as a truly boundary solution technique for 3D thermoelastic analysis of generally anisotropic solids, as a true exact BIE has now been obtained.

Acknowledgement: The authors gratefully acknowledge the financial support from the National Science and Engineering Research Council of Canada and the National Science Council of Taiwan (NSC 102-2221-E-006-290-MY3).

References

Buroni, F. C.; Saez, A. (2010): Three-dimensional Green's function and its derivative for materials with general anisotropic magneto-electro-elastic coupling. *Proceedings of the Royal Society of London- A*, vol. 466, pp. 515-537.

Deb, A.; Banerjee, P. K. (1990): BEM for general anisotropy 2D elasticity using particular integrals. *Communications in Applied Numerical Methods,*, vol. 6, pp. 111-119.

Deb, A.; Henry, Jr. D. P.; Wilson, R. B. (1991): Alternate BEM formulation for 2D and 3D anisotropic thermoelasticity. *International Journal for Numerical Methods in Engineering*, vol. 27, pp. 1721-1738.

Danson, D. (1983): Linear isotropic elasticity with body forces. *in Progress in Boundary Element Methods,* C.A. Brebbis (ed.), Pentech Press, London.

Kogl, M.; Gaul, L. (2003): A boundary element method for coupled thermoelasticity. *Archive of Applied Mechanics*, vol. 73, pp. 377-398.

Lee, V. G. (2003): Explicit expression of derivatives of elastic Green's functions for general anisotropic materials. *Mechanics Research Communications,* vol. 30, pp. 241–249.

Lee, V. G. (2009): Derivatives of the three-dimensional Green's function for anisotropic materials. *International Journal of Solids and Structures,* vol. 46, pp. 1471-1479.

Lifshitz, I. M.; Rozenzweig, L. N. (1947): Construction of the Green tensor for

the fundamental equation of elasticity theory in the case of unbounded elastically anisotropic medium. *Zh. Eksp. Teor. Fiz.*, vol. 17, pp. 783-791.

Nye, J. F. (1960): *Physical Properties of Crystals. Their Representations by Tensors and Matrices*, Clarendon, Oxford.

Partridge, P. W.; Brebbia, C. A.; Wrobel, L. C. (1994): *The Dual Reciprocity Bounadry Element Method.* Computational Mechanics Publications, Southampton, U.K.

Phan, P. V.; Gray, L. J.; Kaplan, T. (2004): On the residue calculus evaluation of the 3D anisotropic elastic Green's function. *Communications in Numerical Methods in Engineering,* vol. 20, pp. 335-341.

Rizzo, F. L.; Shippy, D. J. (1977): An advanced boundary integral equation method for three-dimensional thermoelasticity. *Inernational Journal for Numerical Methods in Engineering,* vol. 11, pp. 1753-1768.

Sales, M. A.; Gray, L. J. (1998): Evaluation of the anisotropic Green's function and its derivatives. *Computers & Structures*, vol. 69, pp. 247-254.

Schclar, N. A. (1994): *Anisotropic Analysis Using Boundary Elements*. Computational Mechanics Publications, Southampton, U.K.

Shiah, Y. C.; Tan, C. L. (1999a): Exact boundary integral transformation of the thermoelastic domain Integral in BEM for general 2D anisotropic elasticity, *Computational Mechanics*, vol. 23, pp. 87-96.

Shiah, Y. C.; Tan, C. L. (1999b): Calculation of interior point stresses in two-dimensional boundary element analysis of anisotropic bodies with body forces. *Journal of Strain Analysis for Engineering Design*, vol. 34, pp. 117-128.

Shiah, Y. C.; Tan, C. L. (2000): Determination of internal point stresses in two dimensional BEM thermoelastic analysis of anisotropic bodies. *International Journal of Solids and Structures*, vol. 37, pp. 809-829.

Shiah, Y. C.; Tan, C. L. (2004): BEM Treatment of Three Dimensional Anisotropic Field Problems by Direct Domain Mapping. *Engineering Analysis with Boundary Elements*, vol. 28, pp. 43-52.

Shiah, Y. C.; Tan, C. L. (2012): Boundary element method for thermoelastic analysis of three-dimensional transversely isotropic solids. *International Journal of Solids and Structures*, vol. 49, pp. 2924–2933.

Shiah, Y. C.; Tan, C. L.; Lee, V. G. (2008): Evaluation of explicit-form fundamental solutions for displacements and stresses in 3D anisotropic elastic solids. *CMES-Computer Modeling in Engineering & Sciences*, vol. 34, no. 3, pp. 205-226.

Shiah, Y. C.; Tan, C. L.; Lee, R. F. (2010): Internal point solutions for displace-

ments and stresses in 3D anisotropic elastic solids using the boundary element method. *CMES-Computer Modeling in Engineering & Sciences*, vol. 69, pp. 167-197.

Tan, C. L.; Shiah, Y. C.; Lin, C. W. (2009): Stress analysis of 3D generally anisotropic elastic solids using the boundary element method. *CMES-Computer Modeling in Engineering & Sciences*, vol. 41, pp. 195-214.

Shiah, Y. C.; Tan, C. L.; Wang, C. Y. (2012a): Efficient Computation of the Green's Function and its Derivatives for Three-Dimensional Anisotropic Elasticity in BEM Analysis. *Engineering Analysis with Boundary Elements*, vol. 36, pp. 1746-1755.

Shiah, Y. C.; Tan, C. L.; Wang, C. Y. (2012b): An Improved Numerical Evaluation Scheme of the Fundamental Solution and its Derivatives for 3D Anisotropic Elasticity Based on Fourier Series. *CMES-Computer Modeling in Engineering & Sciences*, vol. 87, no. 1, pp. 1-22.

Tan, C. L.; Shiah, Y. C.; Wang, C. Y. (2013): Boundary element elastic stress analysis of 3D generally anisotropic solids using fundamental solutions based on Fourier series. *International Journal of Solids and Structures*, vol. 50, pp. 2701-2711.

Ting, T. C. T.; Lee, V. G. (1997): The three-dimensional elastostic Green's function for general anisotropic linear elastic solid. *Quarterly Journal of Mechanics and Applied Mathematics,* vol. 50, pp. 407-426.

Tonon, F.; Pan, E.; Amadei, B. (2001): Green's functions and boundary element method formulation for 3D anisotropic media. *Computers & Structures*, vol. 79, pp. 469-482.

Wang, C. Y.; Denda, M. (2007): 3D BEM for general anisotropic elasticity, *International Journal of Solids and Structures*, vol. 44, pp. 7073-7091.

Wilson, R. B.; Cruse, T. A. (1978): Efficient implementation of anisotropic three dimensional boundary integral equation stress analysis, *Intenrational Journal for Numerical Methods in Engineering,* vol. 12, pp. 1383-1397.

Zhang, J. J.; Tan, C. L.; Afagh, F. F. (1996): A general exact transformation of body-force volume Integral in BEM for 2D anisotropic elasticity. *Computational Mechanics*, vol. 19, pp. 1-10.